# Characterization of carbon nanotubes via the vibrational density of states

Albert J. Pool
Study: Physics and Astronomy

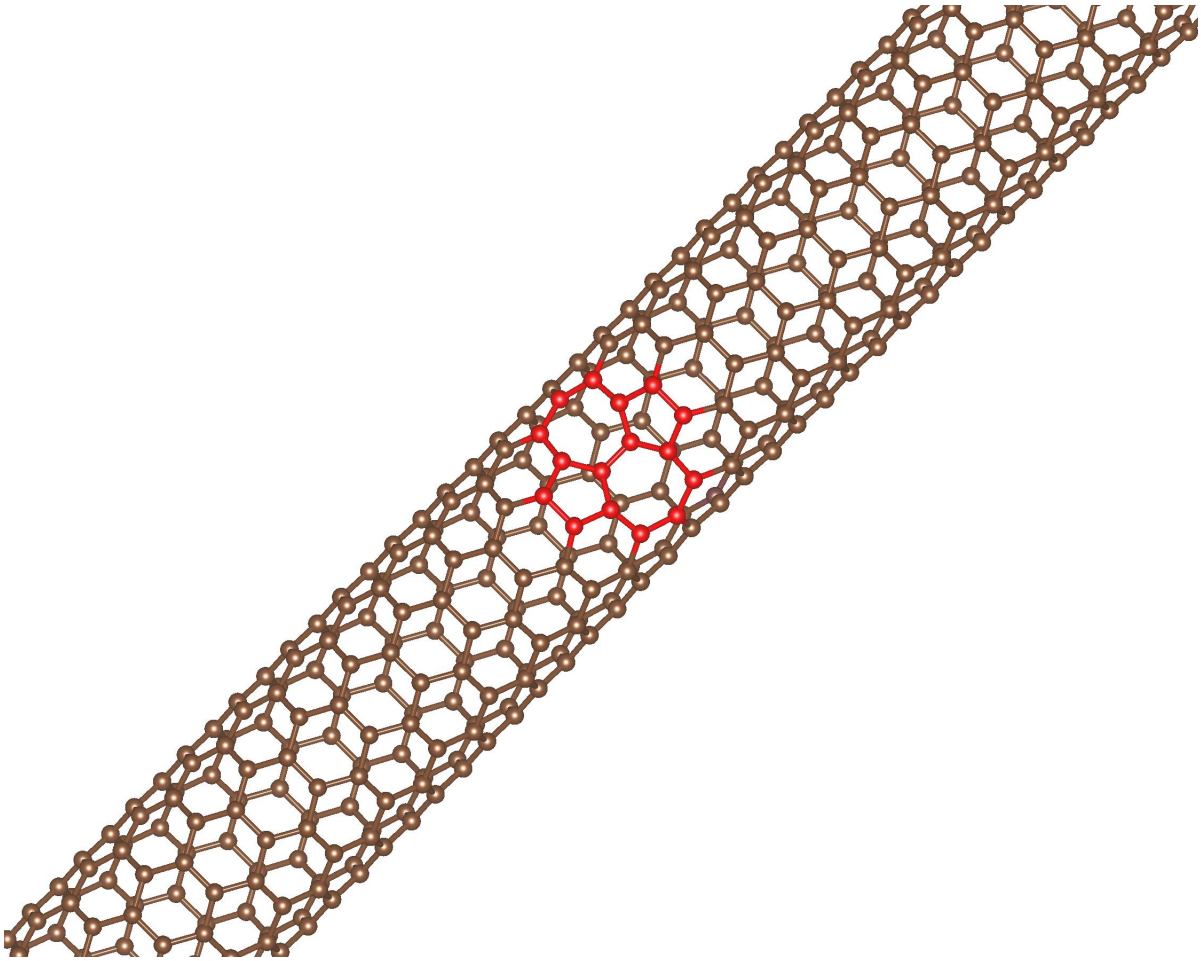

Supervisors:
Prof. Dr. Gerard T. Barkema
Department of Information and Computing Science, Universiteit Utrecht

Sandeep K. Jain
Institute for Theoretical Physics, Universiteit Utrecht

A thesis presented for the degree of Bachelor of Science
January 2017

Universiteit Utrecht

**Abstract**

Carbon nanotubes are a very promising material for future nanoelectronics, batteries, composite materials, and have many more applications. The electrical and chemical properties of carbon nanotubes vary significantly with different chirality and diameter, making the experimental determination of these structural properties important. Here, it is shown that the vibrational density of states (VDOS) contains information on the structure of carbon nanotubes, particularly at low frequencies. It is shown that the diameter and chirality of the nanotubes can be determined from the characteristic low frequency $L$ and $L'$ peaks in the VDOS. For zigzag nanotubes, the $L$ peak splits into two peaks giving rise to another low energy $L''$ peak. The significant changes in the frequencies and relative intensities of these peaks open up a route to distinguish among structurally different nanotubes. A study of Stone–Wales defects of different orientations, and with varying defect density reveals that different structural defects also leave distinct fingerprints in the VDOS, particularly in the $L$ and $L'$ modes. With these results, more structural information can be obtained from experiments which can directly measure the VDOS, such as inelastic electron tunneling spectroscopy and inelastic neutron spectroscopy.

# Contents

# 1 Introduction

Carbon is a very interesting element to study. Due to its valence of 4, many structures, called allotropes, can be formed out of carbon alone. Diamond and graphite are well-known examples of this, but many more exist. In most allotropes except diamond, carbon is found in $sp^2$-hybridised state, which means that it will form three bonds with its neighbors at angles of 120°. In this state, carbon usually forms a hexagonal lattice. Graphite consists of many layers of carbon in such a hexagonal lattice bound together by Van der Waals forces. Graphene, a single layer of one atom thick, was first extracted from graphite in 2004 by Geim and Novoselov [1].

Many graphene-like materials had already been synthesised before graphene itself. In 1985, a spherical molecule of 60 carbon atoms was found, which was named buckminsterfullerene by its discoverers [2]. Since that discovery, a whole class of fullerenes has been found: hollow carbon nanostructures consisting of hexagons and pentagons. In 1991, Iijima observed carbon nanotubes: cylinders of carbon in a hexagonal graphene-like lattice [3]. Whether he was the first to observe carbon nanotubes is a matter of debate [4], but this discovery certainly brought carbon nanotubes to the attention of many scientists, resulting in a lot of theoretical and experimental carbon nanotube research which is still ongoing as more applications of carbon nanotubes keep to be found.

The goal of this work is to present the computer simulation research which I have done on carbon nanotubes, following on the work on graphene by Jain et al. [5].

## 1.1 Carbon nanotubes: characteristics, production and applications

Carbon nanotubes can be seen as a graphene sheet, rolled into a tube. This is possible in many different ways. Carbon nanotubes are characterized by two integer numbers $(n, m)$, describing the chiral vector between two equivalent lattice points on a graphene sheet, which coincide when the sheet is rolled into a tube. In Figure 1, it is shown how this chiral vector can be formed using the unit vectors of the graphene lattice.

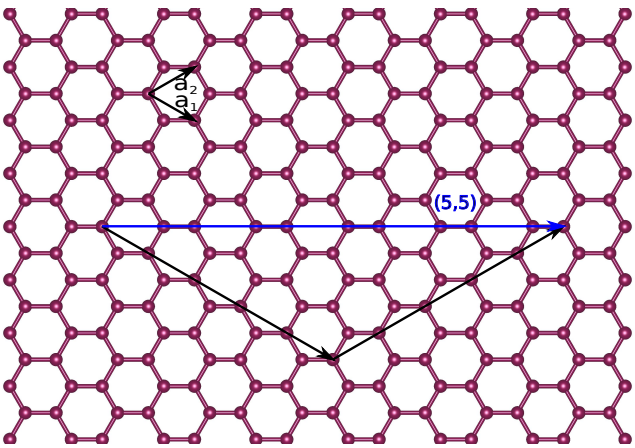


Figure 1: The unit vectors $\vec{a_1}$ and $\vec{a_2}$ of the graphene lattice and the chiral vector of a $(5, 5)$ armchair tube: $5\vec{a_1} + 5\vec{a_2}$. This vector describes which points coincide when a graphene sheet is rolled into a carbon nanotube.

Two important chiralities are armchair $(n, n)$, featuring C–C bonds perpendicular to the tube axis, and zigzag $(n, 0)$, featuring C–C bonds parallel to the tube axis. A nanotube with any other $(n, m)$ chirality is called chiral [6]. Examples of armchair, zigzag and chiral nanotubes can be seen in Figure 2.

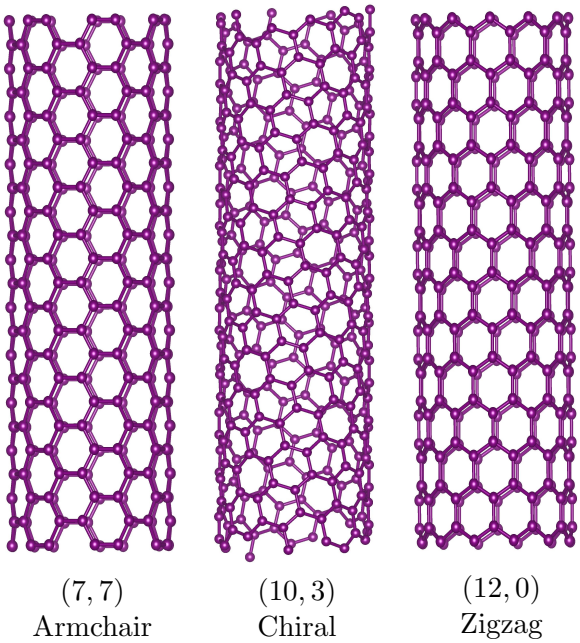


Figure 2: Examples of chiralities of carbon nanotubes.

Carbon nanotubes can be found in a large range of diameters. Nanotubes as small as 4 Å have been found [7], and an upper bound for the diameter of stable carbon nanotubes has been established around 51 Å [8]. In many experiments multi-walled carbon nanotubes have been found, and nanotubes consisting of as much as 18 shells have been imaged with electron microscopy [9]. The usual length of carbon nanotubes is in the order of millimeters [10], but carbon nanotubes of many centimeters long have been produced in experiments with well-controlled growth conditions [11].

The production of carbon nanotubes is possible using various methods, generally starting with a sample of graphitic carbon. The carbon nanotubes observed by Iijima [3] as well as the first mass-produced carbon nanotubes were produced using arc discharge: by igniting an arc between two graphite electrodes in a gas such as argon, carbon is evaporated and condenses to form carbon nanotubes. Using a catalyst material, this process can be tuned to yield single-walled carbon nanotubes.

Another method to produce high quality carbon nanotubes is laser ablation, which has been used for the production of fullerenes: by targeting a graphite target in a stream of helium gas with an intense laser beam, carbon is evaporated. Catalyst particles ensure that it condenses to carbon nanotubes with a narrow diameter distribution.

One of the easiest methods, currently used in many experiments is chemical vapor decomposition (CVD), in which a volatile compound containing carbon is heated and decomposes on the surface of catalyst particles [10]. By tuning the temperature [12] or the catalyst [13], this process can be used to yield carbon nanotubes with a narrow diameter distribution.

**Properties and applications of carbon nanotubes**

Carbon nanotubes have remarkable mechanical and electronic properties. The tensile strength and flexibility of carbon nanotubes are excellent, which allows using them in composite materials [14]. The electronic properties of carbon nanotubes depend on chirality; carbon nanotubes can either be metallic or semiconducting. Metallic carbon nanotubes are those with a chiral index $(n, m)$ where $n-m$ is a multiple of 3; other carbon nanotubes are semiconducting [15, 16, 17], and this distinction is important when applying carbon nanotubes in electronics. Carbon nanotubes are extremely conductive and can carry large current densities [14, 18].

Applications of carbon nanotubes in electronics include the production of smaller transistors than current silicon technology allows [19, 20], flexible integrated circuits [21, 22], conductors for the interconnection of components in nanoelectronics [23], and as an electrode material in improved batteries [24, 25]. Transistor and battery technology are currently limiting factors in the production of electronic devices; the study of carbon nanotube electronics will make way for innovations in this field.

Another interesting application for carbon nanotubes is found in chemical sensors. Carbon nanotubes have been proposed for high-sensitivity gas sensors [26, 27] and sensors for biomolecules [28, 29].

For these applications it is important to be able to distinguish different carbon nanotube chiralities, because of their variation in electronic properties.

**Experimental characterization of carbon nanotubes**

It is currently possible in experiments to identify a single carbon nanotube by its diameter and chiral angle as measured by direct local techniques such as atomic resolution scanning tunneling microscopy (STM) [16], transmission electron microscopy (TEM) [30, 31], and electron diffraction [32, 33]. As these microscopy techniques are rather expensive, indirect methods for characterization heave been developed, such as Raman spectroscopy [34], and photoluminescence excitation spectroscopy [35, 36, 37]. Very recently, the determination of chiral indices of two- or three-walled carbon nanotubes by a combination of electron diffraction and Raman spectroscopy has been reported [38].

**Defects in carbon nanotubes**

In experimentally produced carbon nanotubes, intrinsic defects commonly occur. A common defect is the Stone–Wales (SW) defect which is formed by the rotation of a C–C bond by 90° [39, 40]. This rotation results in two pentagons and two heptagons in the otherwise hexagonal lattice. A drawing of a Stone–Wales defect can be seen in Figure 3.

This SW defect is a common defect in graphene [41]. In carbon nanotubes, it has an even lower formation energy, especially in tubes with smaller diameters [42], which makes it an important defect to study. SW defects have direct consequences on the electrical [43], mechanical [44, 45, 46], and chemical [47, 48] properties of carbon nanotubes. The SW defect is considered to form spontaneously as a result of excess strain [49, 50], and is suggested to be responsible for plastic deformation of carbon nanotubes [51].

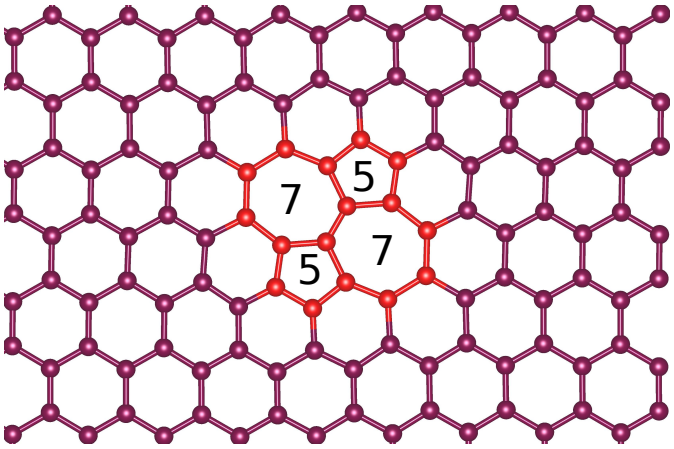


Figure 3: A Stone–Wales defect in a graphene sheet, with the numbers indicating pentagons and heptagons.

This defect can be considered as a dislocation dipole: further rotation of C–C bonds separates it into two dislocation cores both consisting of a pentagon and a heptagon [52]. Other nanotubes with topological defects, for instance containing octagons, have also been reported [49].

Other types of defects in carbon nanotubes include vacancies, which show a stronger effect on the strength of a carbon nanotube [53]. Vacancy defects are commonly formed by irradiation and can survive for macroscopic times at room temperature; but as a vacancy is metastable, atoms will rearrange to mend the defect [54, 55].

Carbon nanotubes can also contain heteroatoms: atoms from elements other than carbon. Common hetero-atom dopants experimentally integrated into the graphene lattice include nitrogen and boron. Due to the different electrical and chemical properties of doped carbon nanotubes, applications are suggested in chemistry and energy storage devices [56]. It is also possible for foreign atoms or molecules to be adsorbed to the carbon nanotube surface; for many molecules adsorption occurs most strongly at defect sites [48, 57]. This effect is studied to use carbon nanotubes as chemical sensors [48, 27].

**Why simulations?**

Computer simulation is a powerful tool in carbon nanotube research. By simulations, the properties can be predicted of carbon nanotubes of any chirality or any number of defects: many different nanotubes can be studied without having to synthesize every single one of them. A common and frequently used method to simulate carbon nanotubes is density-functional theory (DFT). However, DFT is computationally intensive and therefore limits the size of the system that can be studied [58, 59]. Because the study of vibrational properties requires simulation of systems larger than a few hundred atoms, DFT is not a suitable technique here. A semiempirical potential was used instead: a simplified model describing the behavior of a carbon molecule, with parameters determined by DFT calculations. This allows to study much larger systems in far less computation time. Semiempirical potentials for carbon nanotubes have recently been shown to correspond fairly well with experiments [60, 61].

## 1.2 Vibrational density of states

The vibrational density of states (VDOS) can well be used to determine many chemical and physical properties of carbon nanotubes. Besides studying chirality and defects, the VDOS can also be used to calculate thermal conductivity [62]. There are different ways to determine the VDOS experimentally. Raman spectroscopy allows measuring certain Raman active vibrational modes [63, 64, 65] and has been used to study many carbon nanotube properties such as chirality and defects [34, 39, 65, 66, 67, 68]. It is possible to study the full vibrational spectrum in experiments by inelastic neutron scattering [69, 65], or inelastic electron tunneling spectroscopy (IETS) [70]. IETS can also be used for localized measurements using the tip of an STM (STM-IETS), which allows study of local properties such as defects, different tubes joined together, or tube caps [71, 72]. The vibrational spectrum of graphene has already been experimentally mapped with IETS [73], and this opens up a possibility to use the same technique to characterize carbon nanotubes.

Using the same semiempirical potential, the VDOS of graphene depending on the number of defects has already been studied [5]. As a carbon nanotube can be seen as a graphene sheet rolled into a tube, it is expected that the VDOS of a carbon nanotube will approach that of graphene in the limit of large diameter. The effect of defects is expected to be comparable, with the prominent peaks in the spectrum becoming weaker. However in the case of carbon nanotubes, there are various different chiralities to be studied and in each of them, multiple defect orientations are possible. In this work, the vibrational properties will be reported for a selection of carbon nanotubes which allows studying the dependence of the VDOS on the diameter and chiral angle and provides insight into the effects of different defect orientations on the VDOS.

## 2 Computational method

To study the defect mechanics and vibrational properties of a carbon nanotube, a semiempirical potential recently developed for graphene was used [74]. Apart from the already mentioned VDOS of graphene, this potential has also been used effectively to study twisted bilayer graphene [75], the effect of boundary conditions in graphene samples [76], and graphene nanobubbles [77].

In this method, the potential of a system of carbon atoms is given by the following expression:

$$E = \frac{3}{16}\frac{\alpha}{d^2}\sum_{i,j}(r_{ij}^2 - d^2)^2 + \frac{3}{8}\beta d^2 \sum_{j,i,k}\left(\theta_{jik} - \frac{2\pi}{3}\right)^2 + \gamma \sum_{i,jkl} r_{i,jlk}^2. \tag{1}$$

Here, $r_{ij}$ is the length of the bond between two atoms $i$ and $j$, $\theta_{jik}$ the angle between the two bonds connecting atom $i$ to $j$ and $k$, respectively, and $r_{i,jkl}$ the distance between atom $i$ and the plane formed by its three neighboring atoms $j$, $k$, and $l$. The parameters $\alpha = 26.060$ eV/Å$^2$, $\beta = 5.511$ eV/Å$^2$, $\gamma = 0.517$ eV/Å$^2$, and $d = 1.420$ Å are used, which were obtained by density-functional theory (DFT) calculations for graphene [74].

This equation is applied to a system of carbon atoms connected together. Because the potential does not allow for dangling bonds or atoms of other species, a periodic boundary condition is used in the direction of the tube axis. This means atoms at the top and bottom of the tube are connected together. Another possible option in simulations is to put caps on the simulated tube, but this would introduce unwanted effects from the caps when studying vibrational properties; periodic boundary conditions are in this case the best approximation of a macroscopically large tube. The boundary condition is force-free: the size of the simulated system is allowed to change under forces between atoms on both sides of the edge.

The forces on the atoms in the system are calculated by taking the derivative of the energy with respect to the coordinates of the atoms. The system is relaxed by to its lowest-energy state by iteratively moving the atoms into the direction of the force until the force is zero.

**Determining the vibrational density of states**

Starting with a carbon nanotube in its lowest-energy state, the second derivatives of the energy were calculated with respect to the $x$-, $y$-, and $z$-coordinates of all atoms by slightly displacing an atom and calculating the resulting force on all atoms. Because of the angular term in (1), this does not only include neighbors of the atom but also neighbors of neighbors. For a system of $N$ atoms, the result is a $3N \times 3N$ matrix called the Hessian matrix.

From the Hessian matrix the vibrational modes of the system can be derived by diagonalization. The eigenvalues of this matrix represent the force constants of the vibrational modes in eV/Å$^2$, and the eigenvectors represent the normal coordinates of the vibrational modes. These force constants $k$ are converted into frequencies as:

$$f = \frac{1}{2\pi c}\sqrt{\frac{k}{m}}. \tag{2}$$

Here, $c$ is the speed of light and $m = 1.99 \times 10^{-26}$ kg the mass of a carbon atom. This results in $3N$ vibrational modes, including three translational modes and one rotational mode around the axis, which can be recognized by their force constants which are zero. The VDOS is now the density of vibrational modes as a function of frequency. To plot the VDOS, the energies of the vibrational modes are taken and convoluted with a Gaussian function with a width of $\sigma = 14$ cm$^{-1}$.

The semiempirical potential above allows studying the VDOS of systems with hundreds of atoms without much computational effort. This is crucial for determining the VDOS; calculations on smaller systems are only able to determine a limited number of modes, and the resulting VDOS would only be a crude approximation of the VDOS of a macroscopic carbon nanotube.

# 3 Results

## 3.1 Armchair nanotubes

The vibrational spectrum of various armchair nanotubes of different diameters ($D$) has been calculated and compared with the VDOS of graphene by Jain et al. [5] as shown in figure 4. It can be seen that the small diameter tube $(5, 5)$ has high frequencies for the $L$ and $L'$ modes; there is a shift towards lower frequencies as the diameter of the tubes increases and converges to the values of graphene in infinite diameter limit. The VDOS of three armchair nanotubes and graphene has been plotted as shown in figure 4(a). The frequencies of the $L$ and $L'$ peaks for many armchair tubes as a function of $(n, n)$ chiral index, and as a function of inverse tube diameter are shown in figure 4(b) and figure 4(c), respectively. For figure 4(c), the diameter $D$ of an $(n, m)$ tube is computed using

$$D = \frac{\sqrt{3}}{\pi} d \sqrt{n^2 + nm + m^2}, \tag{3}$$

with $d = 1.420$ Å, the ideal C–C bond length [6].

At high frequencies, the VDOS is very similar to that of graphene but the variation occurs in the low frequency range ($0 - 600$ cm$^{-1}$). It is apparent that the $L$ and $L'$ peaks shift towards a lower frequency as a function of increasing diameter. The frequency of the $L$ peak for the smallest diameter $(5, 5)$ tube ($D = 6.78$ Å) is around 99% higher compared to that of graphene but rapidly decreases to 31% for the $(10, 10)$ tube ($D = 13.56$ Å) and 15% for the $(15, 15)$ tube ($D = 20.34$ Å). The variation in the frequency of the $L'$ peak is even more prominent compared to graphene as the values are: 240% for the $(5, 5)$ tube, 89% for the $(10, 10)$ tube and 34% for the $(15, 15)$ tube. There is a significant decrease in the intensities of both $L$ and $L'$ peaks as a function of decreasing diameter. The intensity of the $L$ peak decreases by 5% for the $(15, 15)$ tube, 12% for the $(10, 10)$ tube, and 28% for the $(5, 5)$ tube, compared to bulk graphene. Similarly, the intensity of $L'$ peak decreases by 5% for the $(15, 15)$ tube, 11% for the $(10, 10)$ tube, and 19% for the $(5, 5)$ tube, compared to bulk graphene.

To further characterize these two low energy vibrational modes, vibrational modes found in the $L$ and $L'$ peaks have been plotted in figure 4(d) and figure 4(e), respectively. One of the vibrational modes in the $L'$ peak is the radial breathing mode (RBM), a Raman active mode for which the frequency has been determined experimentally for many carbon nanotubes [65, 78]. The radial breathing mode frequency is given by Maultzsch et al. [78] as

$$\omega_{RBM} = \frac{c_1}{D} + c_2, \tag{4}$$

with experimentally determined constants $c_1 = 215 \pm 2$ cm$^{-1}$nm and $c_2 = 18 \pm 2$ cm$^{-1}$, and $D$ is determined by eq. (3). It is interesting to note that the position of the $L'$ peak in armchair nanotubes complies almost exactly with this experimental radial breathing mode frequency, as seen in figure 4(c). This observation further validates the numerical results presented here.

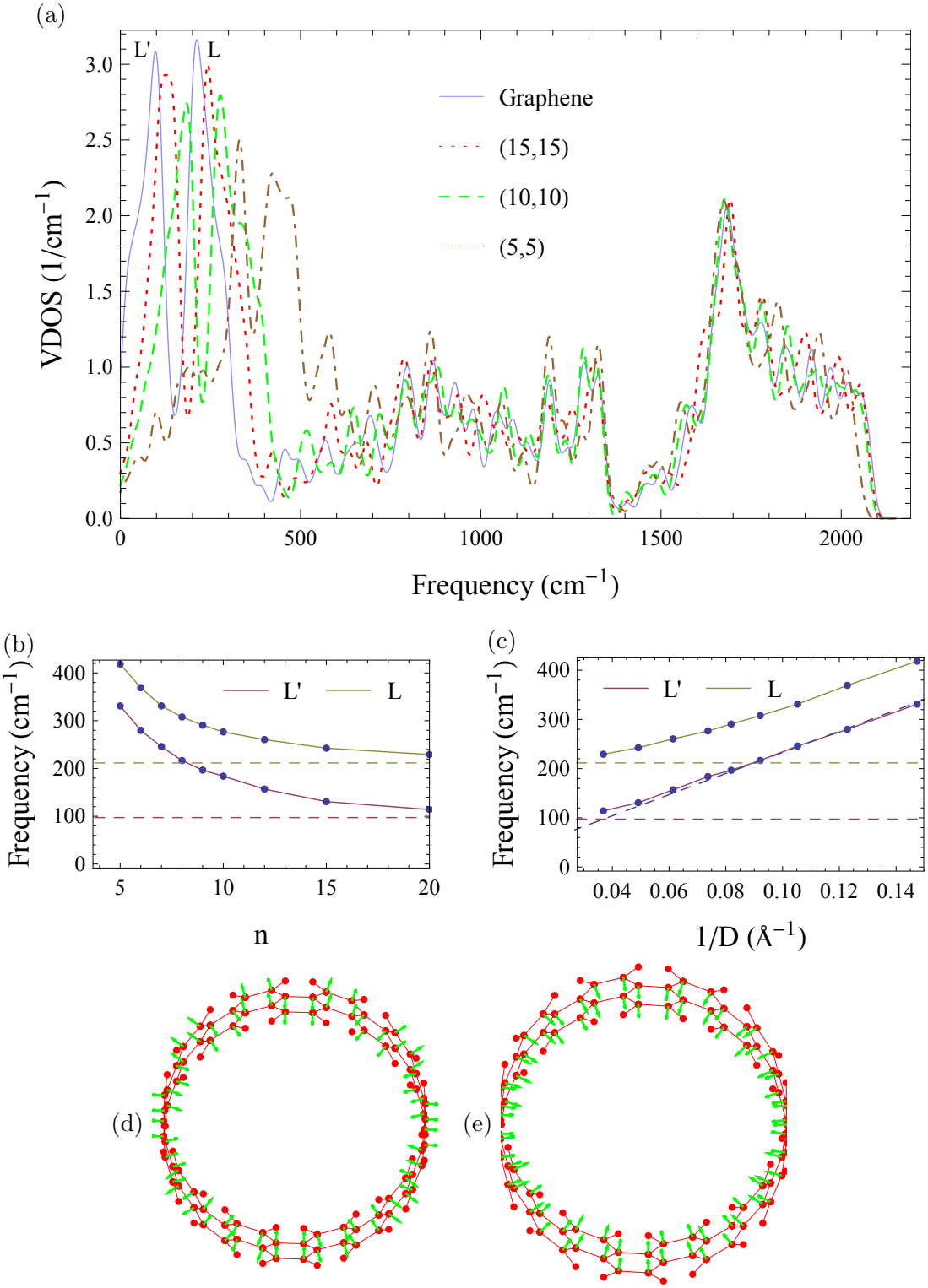


Figure 4: Dependence of VDOS for armchair carbon nanotubes on the diameter $D$. (a) VDOS of three armchair nanotubes compared to graphene. (b) Position of $L$ and $L'$ peaks as a function of chiral index $n$ for nanotubes with chirality $(n, n)$ . Dashed lines are for graphene. (c) Position of $L$ and $L'$ peaks as a function of inverse tube diameter, with the radial breathing mode frequency from eq. (4) shown in dashed blue. (d) One of the vibrational modes in the $L$ peak of a $(10, 10)$ nanotube. Here, red dots are carbon atoms in the nanotube and green arrows are corresponding vibrational displacements. (e) The radial breathing mode in the $L'$ peak of a $(10, 10)$ nanotube.

### 3.2 Zigzag nanotubes

The vibrational spectrum of various zigzag nanotubes of different diameters has been calculated and compared with the VDOS of graphene as shown in figure 5. Interestingly, there are three, rather than two distinct low frequency peaks visible for $n \lesssim 20$ tubes. In these small diameter zigzag tubes ($D \lesssim 15$ Å), the $L$ peak splits into two: the one with the lower frequency has been labeled $L''$. It can again be seen that the small diameter tube $(10, 0)$ has high frequencies for the $L$ and $L'$ modes and there is a shift towards higher frequencies as the diameter of the tubes increases; it converges to the values of graphene in the infinite diameter limit. The VDOS of three zigzag nanotubes and graphene has been plotted in figure 5(a). Figure 5(b) and figure 5(c) show the frequencies of the $L$, $L'$, and $L''$ peaks for many zigzag tubes as a function of $(n, 0)$ chiral index, and as a function of inverse tube diameter, respectively.

At high frequencies, the VDOS is very similar to that of graphene but the variation occurs in the low frequency range ($0 - 600$ cm$^{-1}$). It is clear that the $L$ and $L'$ peaks shift towards a lower frequency as a function of increasing diameter. The frequency of the $L$ peak for the smallest diameter $(10, 0)$ tube ($D = 7.83$ Å) is around 104% higher compared to that of graphene but rapidly decreases to 12% for the $(30, 0)$ tube ($D = 23.48$ Å). The intensity of this peak decreases by 10% for the $(30, 0)$ tube, to 36% for the $(10, 0)$ tube compared to graphene. The variation in the frequency of the $L'$ peak is even more prominent as the values are: 114% for the $(10, 0)$ tube, 44% for the $(20, 0)$ tube and 18% for the $(30, 0)$ tube. There is a significant decrease in the intensities of the $L'$ peak as a function of decreasing diameter. The intensity of the $L'$ peak decreases by 2% for the $(30, 0)$ tube, 12% for the $(20, 0)$ tube, and 37% for the $(10, 0)$, compared to bulk graphene.

### 3.3 Chiral nanotubes

It is now clear that diameter has a large influence on the low frequency vibrational spectrum of a carbon nanotube. In both armchair and zigzag, these results can be used to characterize the diameter of carbon nanotubes using the VDOS. The effect of chiral angle on the VDOS can be studied by comparing the VDOS of carbon nanotubes with a comparable diameter and different chiral angle. To achieve this, the armchair $(7, 7)$, chiral $(10, 3)$ and zigzag $(12, 0)$ nanotubes have been used, which have diameters of 9.49 Å, 9.23 Å, and 9.39 Å respectively. The VDOS of these three nanotubes is visible in figure 6.

Figure 6(a) shows, as expected, that there is a significant difference in the low frequency part of the VDOS of these carbon nanotubes of equal diameter with different chiral angles. For the armchair $(7, 7)$ tube, there are two prominent low energy $L$ and $L'$ peaks; but as the chirality changes from armchair to zigzag the $L$ peak splits into two, giving rise to the $L''$ peak. Comparing the $L$ and $L''$ peaks of the chiral $(10, 3)$ and zigzag $(12, 0)$ nanotubes to the $L$ peak of the armchair $(7, 7)$ nanotube, it was found that the frequency of the $L$ peak is 17% higher for the $(10, 3)$ nanotube and 19% for the $(12, 0)$ nanotube, and the frequency of the $L''$ peak is 6% lower for the $(10, 3)$ nanotube and 9% lower for the $(12, 0)$ nanotube. Compared to the $(7, 7)$ nanotube, the frequency of the $L'$ peak is 8% lower for the $(10, 3)$ nanotube and 25% lower

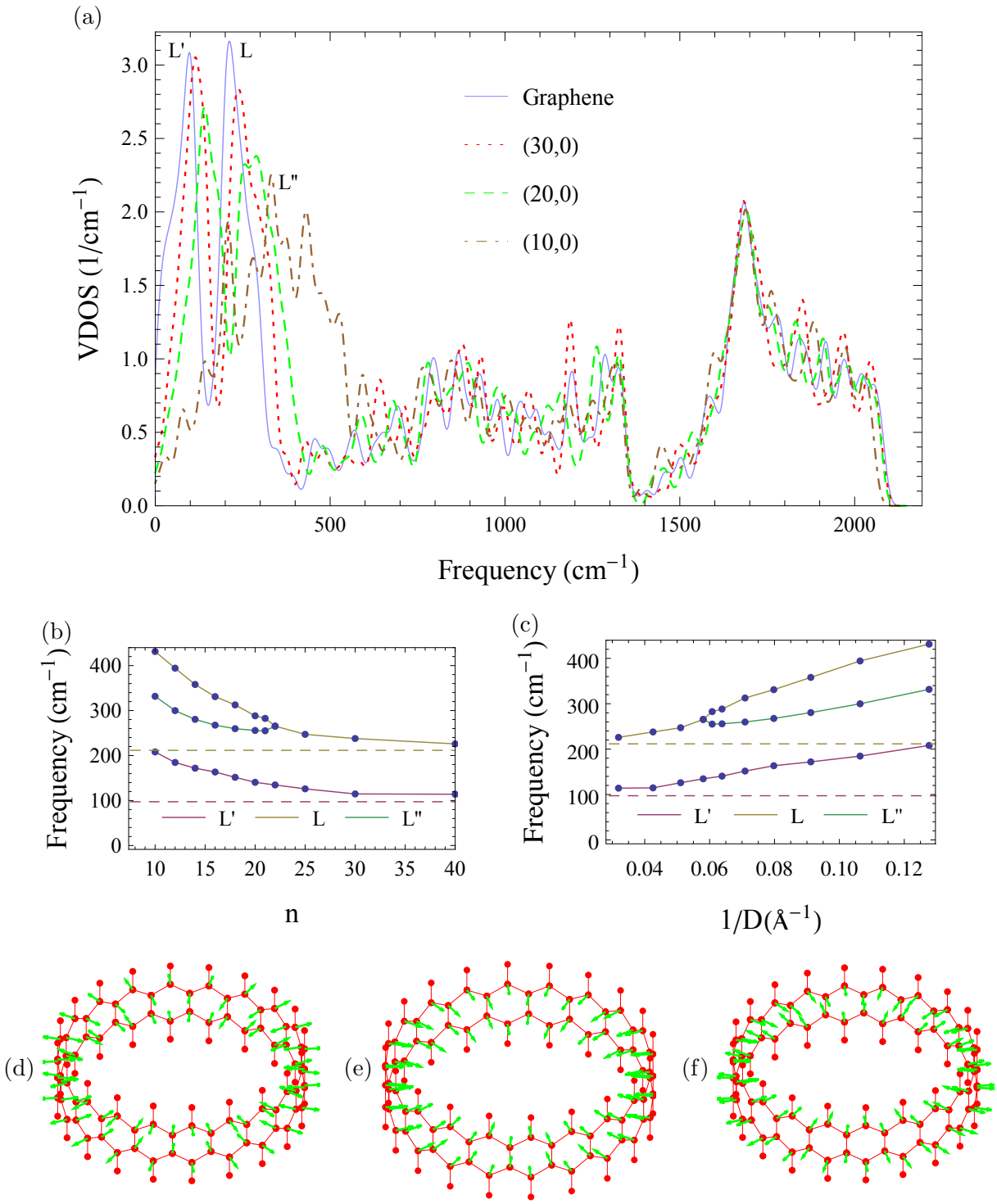


Figure 5: Dependence of VDOS for zigzag carbon nanotubes on the diameter $D$.(a) VDOS of three zigzag nanotubes compared to graphene. (b) Position of $L$, $L'$ and $L''$ peaks as a function of chiral index $n$ for nanotubes with chirality $(n, 0)$. Dashed lines are for graphene. (c) Position of $L$, $L'$ and $L''$ peaks as a function of inverse tube diameter. (d) One of the vibrational modes found in the $L$ peak of a $(20, 0)$ nanotube. Here, red dots are carbon atoms in the nanotube and green arrows are corresponding vibrational displacements. (e) The radial breathing mode in the $L'$ peak of a $(20, 0)$ nanotube. (f) One of the vibrational modes found in the $L''$ peak of a $(20, 0)$ nanotube.

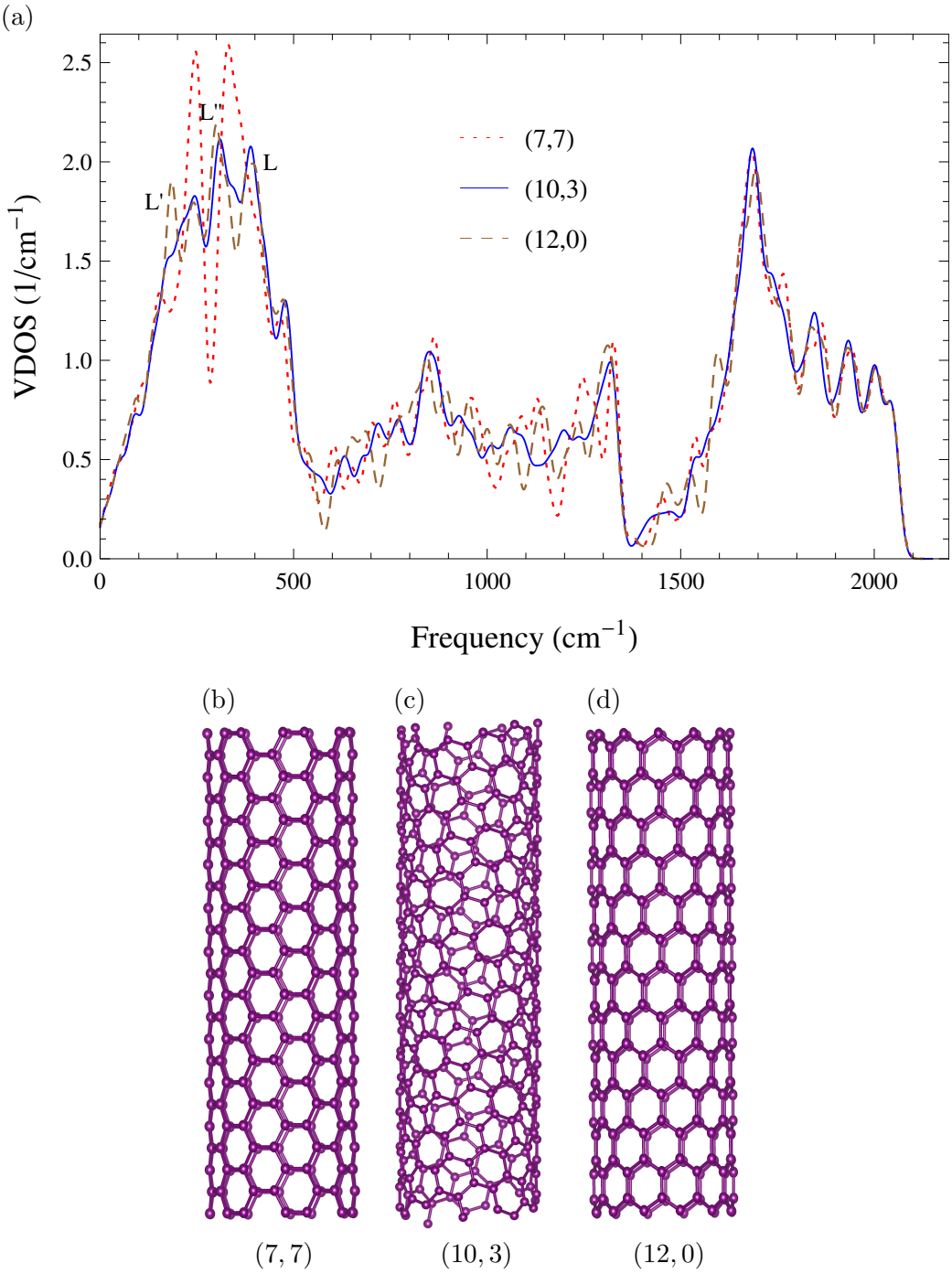


Figure 6: Dependence of VDOS on chiral angle for different chiral tubes with almost the same diameter ($D \sim 9.4$ Å). (a) VDOS of three nanotubes: armchair $(7,7)$, chiral $(10,3)$ and zigzag $(12,0)$. (b-d) For illustration, the three chiralities of nanotubes used in (a).

for the $(7,7)$ nanotube. The effect of the chiral angle on the intensities of these low frequency modes is also very prominent. The intensity of the $L$ peak is 20% lower for the $(10,3)$ nanotube and 23% for the $(12,0)$ nanotube, and the intensity of the $L''$ peak is 18% lower for the $(10,3)$ nanotube and 16% for the $(12,0)$ nanotube. The intensity of the $L'$ peak is 28% lower for the $(10,3)$ nanotube and 26% for the $(12,0)$ nanotube. Therefore these significant changes in the frequencies and intensities of the $L$ and $L'$ peaks in the VDOS can be used to characterize the chirality of carbon nanotubes independent of the diameter.

### 3.4 Stone–Wales defects

The effect of point defects such as Stone–Wales (SW) defects on the VDOS has been studied in two types of nanotubes: armchair $(10,10)$ and zigzag $(20,0)$, which have diameters of 13.56 Å and 15.43 Å, respectively. An SW defect is formed by the rotation of a C–C bond by 90° in a crystalline tube. In general, bonds of three different orientations are found in a carbon nanotube. In the case of armchair and zigzag chiralities, this reduces to two as two types of bonds are equal by symmetry.

**Defects in armchair nanotubes**

In armchair tubes, every carbon atom is connected to one circumferential and two equivalent axial bonds, thus the possible SW defects are obtained by either circumferential bond rotation (CBR) or axial bond rotation (ABR) [79]. The VDOS of a $(10,10)$ carbon nanotube has been calculated with one to four evenly spaced SW defects of both kinds (CBR and ABR) as shown in figure 7.

It can be observed in the $(10,10)$ armchair nanotube with CBR SW defects, that the intensity of the $L$ and $L'$ peaks decreases systematically with an increasing number of SW defects compared to the pristine tube. The intensity of the $L$ peak decreases by $\sim 5\%$ for one SW defect to $\sim 13\%$ for four SW defects as shown in figure 7(g). Similarly the intensity of the $L'$ peak also decreases simultaneously by $\sim 6\%$ for one SW defect to $\sim 14\%$ for four SW defects. For ABR SW defects in an armchair tube, the intensity of the $L$ peak decreases by $\sim 11\%$ for one SW defect and saturates at 13% with a further increase in the number of defects as shown in figure 7(h). But at the same time, the intensity of the $L'$ peak decreases by $\sim 9\%$ for one SW defect to $\sim 14\%$ for three defects, and further decreases to $\sim 15\%$ for four SW defects. For CBR SW defects in armchair tube, the frequency of both peaks does not change significantly as the defect density changes. But in the case of ABR SW defects, there is a minor decrease in the frequencies of the $L$ and $L'$ peaks. The frequency of the $L$ peak decreases by $\sim 2\%$ for one SW defect to $\sim 5\%$ for four SW defects. The frequency of the $L'$ peak decreases by $\sim 4\%$ for one SW defect to $\sim 14\%$ for four SW defects.

**Defects in zigzag nanotubes**

In zigzag nanotubes, every carbon atom is connected to one axial bond and two circumferential bonds, again leading to two possible configurations of SW defects (ABR and CBR). The VDOS as a function of SW defect density has been calculated for both types of defects in a $(20,0)$

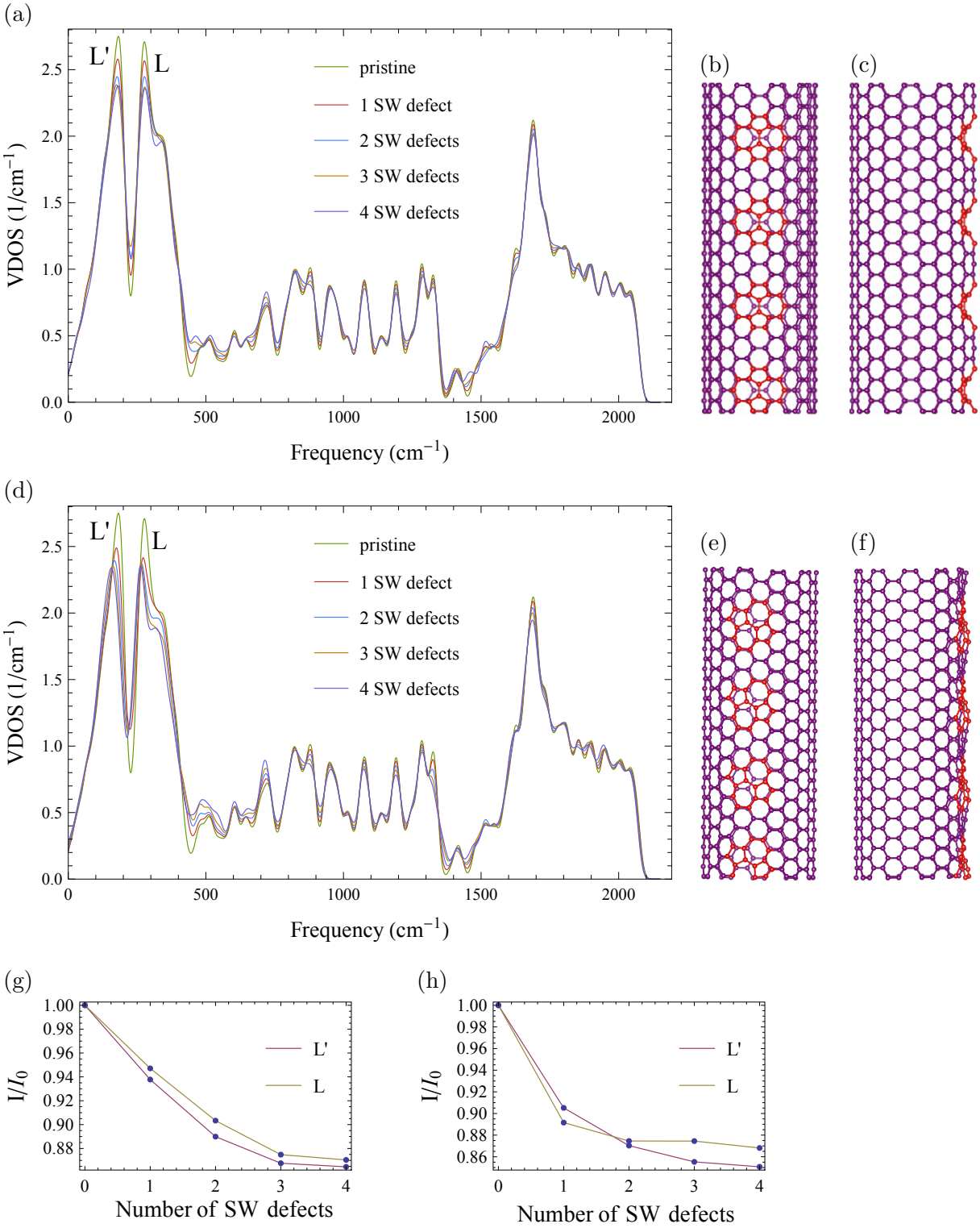


Figure 7: VDOS of armchair $(10, 10)$ tube with one to four evenly spaced Stone–Wales defects. (a) VDOS for circumferential bond rotation (CBR) SW defect in armchair $(10, 10)$ tube with different numbers of defects. (b) Front view of the tube with four SW defects. (c) Side view of the same tube. (d) VDOS for axial bond rotation (ABR) SW defect in armchair $(10, 10)$ tube with different numbers of defects. (e) Front view of the tube with four SW defects. (f) Side view of the same tube. (g) Relative intensity of $L$ and $L'$ peaks as a function of number of CBR SW defects. (h) Relative intensity of $L$ and $L'$ peaks as a function of number of ABR SW defects.

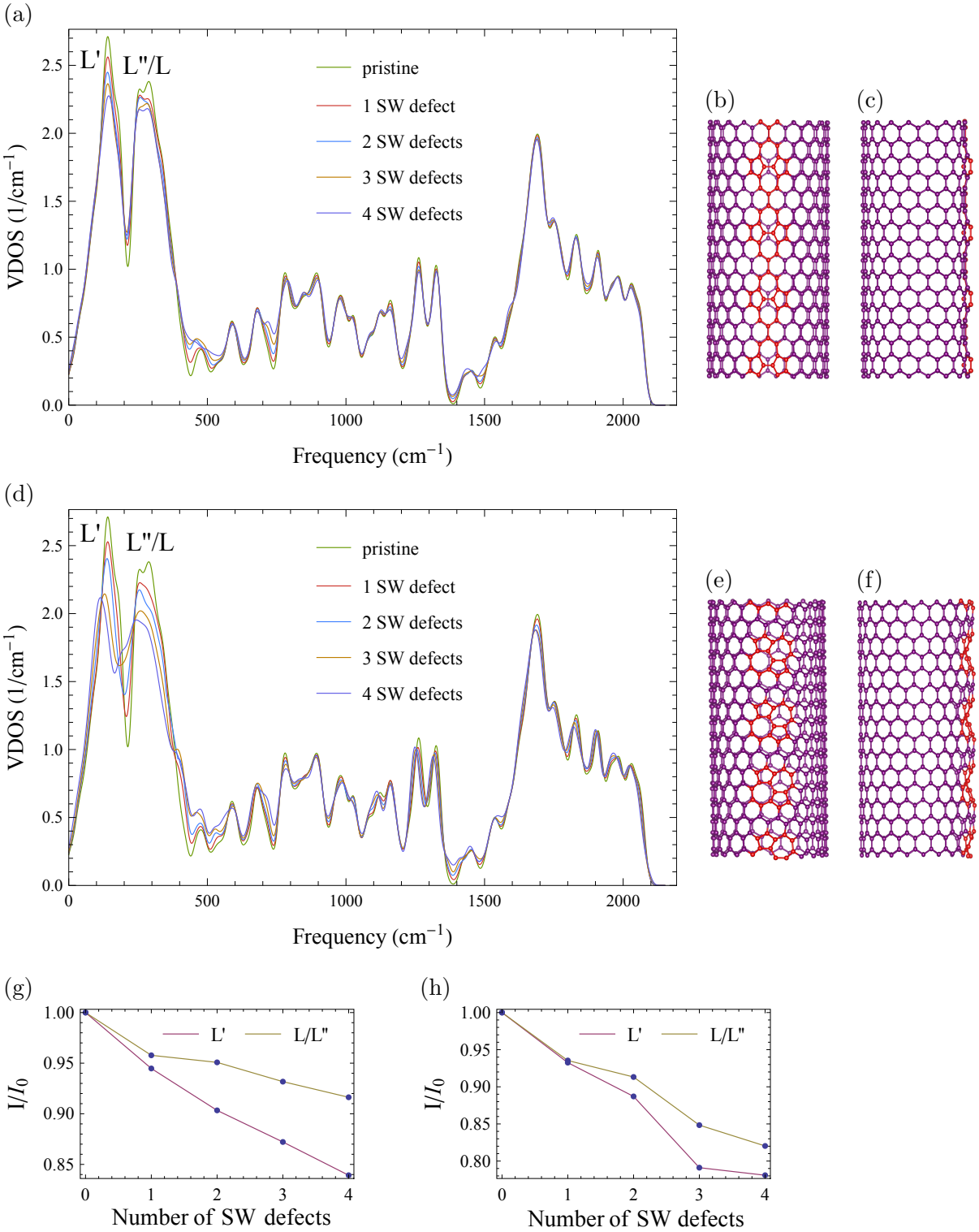


Figure 8: VDOS of zigzag $(20, 0)$ tube with one to four evenly spaced Stone–Wales defects. (a) VDOS for circumferential bond rotation (CBR) SW defect in zigzag $(20, 0)$ tube with different numbers of defects. (b) Front view of the tube with four SW defects. (c) Side view of the same tube. (d) VDOS for axial bond rotation (ABR) SW defect in zigzag $(20, 0)$ tube with different numbers of defects. (e) Front view of the tube with four SW defects. (f) Side view of the same tube. (g) Relative intensity of $L/L''$ and $L'$ peaks as a function of number of CBR SW defects. (h) Relative intensity of $L/L''$ and $L'$ peaks as a function of number of ABR SW defects.

zigzag tube and is shown in figure 8. In figure 8(a) and (d) it can be seen that the $L$ and $L''$ peaks almost merge into a single peak for this tube. As the defect density increases, the distinction between these two peaks becomes even more unclear therefore only the maximum of the intensities of both $L$ and $L''$ peaks has been plotted in the intensity plots in figure 8(g) and (h).

It can be seen that in the $(20, 0)$ zigzag nanotube with CBR SW defects, the intensity of the $L/L''$ and $L'$ peaks decreases systematically with an increasing number of SW defects compared to the pristine tube. The intensity of $L/L''$ peak decreases by $\sim 4\%$ for one SW defect to $\sim 8\%$ for four SW defects as shown in figure 8(g). The intensity of the $L'$ peak decreases more rapidly from $\sim 6\%$ for one SW defect to $\sim 16\%$ for four SW defects. For ABR SW defects in this zigzag tube, the intensity of the $L/L''$ peak decreases by $\sim 6\%$ for one SW defect to a significant 18% for four SW defects as shown in figure 8(h). But at the same time, the intensity of the $L'$ peak also decreases by $\sim 7\%$ for one SW defect to $\sim 21\%$ for three defects, and further decreases to $\sim 22\%$ for four SW defects. As in the case in armchair tubes, the frequencies of both peaks do not change with change in defect density in zigzag tubes with CBR SW defects. But in the case of ABR SW defects, there is a minor decrease in the frequency of the $L'$ peak. The frequency of the $L'$ peak decreases by $\sim 2\%$ for two SW defects to $\sim 19\%$ for four SW defects. This effect is stronger in the $(20, 0)$ zigzag tube compared to the $(10, 10)$ armchair tube. As such, it appears that axial bond rotation in a zigzag nanotube is the defect with the largest influence on the VDOS.

# 4 Conclusion and outlook

In conclusion, it is clear that the vibrational density of states can be used to characterize the structure of carbon nanotubes. With the help of a semiempirical potential, the vibrational spectrum of various carbon nanotubes has been calculated and the characteristic low frequency $L$ and $L''$ modes have been studied. It appears that the high frequency VDOS ($\geq 600$ cm$^{-1}$) of carbon nanotubes is almost identical to that of graphene, but there are significant differences in the low frequency VDOS. By numerical simulations the Raman active radial breathing mode has been identified as the $L'$ peak in the VDOS of armchair nanotubes. Both low frequency $L$ and $L''$ peaks show a shift towards lower frequencies as the diameter of the nanotube increases, and the values of the frequencies converge to that of graphene in the infinite diameter limit.

The results suggest that an $L$ peak in the VDOS with a frequency over 400 cm$^{-1}$, indicates a diameter $\lesssim$ 8 Å. For nanotubes with a diameter $\lesssim$ 15 Å, two sharp peaks close to each other in the low frequency range indicate an armchair chirality of the tube. When the two peaks are further apart and an extra third peak $L''$ peak appears in between, the tube can be characterized as chiral or zigzag nanotube. An $L$ peak with a frequency about twice that of the $L'$ peak, indicates a zigzag chirality.

The effect of point defects such as the Stone–Wales defect on the vibrational spectrum of the nanotubes has been studied as a function of defect density. Increasing the density of Stone–Wales defects leads to broader and less intense peaks, depending on the orientation of the defect with respect to the tube axis. For axial bond rotation there is a slight shift in the frequency of the $L'$ peak for both armchair and zigzag tubes.

This work has resulted in a manuscript which is currently under review [80]. I hope that these results will be useful for further research on carbon nanotubes and their vibrational properties, for instance using inelastic electron tunneling spectroscopy and neutron scattering spectroscopy. Other possibilities for future research include vibrational properties of other carbon structures such as multi-walled carbon nanotubes. Due to their many applications, some of which have been described in the introduction of this work, I expect carbon nanotubes to be important in scientific research for many more years.


# Acknowledgements

I would like to thank my supervisors prof. dr. Gerard Barkema, and PhD student Sandeep Jain, for helping me throughout this process.

## References


[1] K. S. Novoselov, A. K. Geim, S. V. Morozov, D. Jiang, Y. Zhang, S. V. Dubonos, I. V. Grigorieva, and A. A. Firsov, "Electric field effect in atomically thin carbon films," *Science*, vol. 306, no. 5696, pp. 666–669, 2004.

[2] H. W. Kroto, J. R. Heath, S. C. O'Brien, R. F. Curl, R. E. Smalley, *et al.*, "C 60: buckminsterfullerene," *Nature*, vol. 318, no. 6042, pp. 162–163, 1985.

[3] S. Iijima *et al.*, "Helical microtubules of graphitic carbon," *Nature*, vol. 354, no. 6348, pp. 56–58, 1991.

[4] M. Monthioux and V. L. Kuznetsov, "Who should be given the credit for the discovery of carbon nanotubes?," *Carbon*, vol. 44, no. 9, pp. 1621–1623, 2006.

[5] S. K. Jain, V. Juričić, and G. T. Barkema, "Probing crystallinity of graphene samples via the vibrational density of states," *J. Phys. Chem. Lett.*, vol. 6, no. 19, pp. 3897–3902, 2015.

[6] M. S. Dresselhaus, G. Dresselhaus, and P. C. Eklund, *Science of fullerenes and carbon nanotubes: their properties and applications.* Academic Press, 1996.

[7] T. Hayashi, Y. A. Kim, T. Matoba, M. Esaka, K. Nishimura, T. Tsukada, M. Endo, and M. S. Dresselhaus, "Smallest freestanding single-walled carbon nanotube," *Nano Lett.*, vol. 3, no. 7, pp. 887–889, 2003.

[8] M. He, J. Dong, K. Zhang, F. Ding, H. Jiang, A. Loiseau, J. Lehtonen, and E. I. Kauppinen, "Precise determination of the threshold diameter for a single-walled carbon nanotube to collapse," *ACS Nano*, vol. 8, no. 9, pp. 9657–9663, 2014.

[9] L.-C. Qin, X. Zhao, K. Hirahara, Y. Miyamoto, Y. Ando, and S. Iijima, "Materials science: The smallest carbon nanotube," *Nature*, vol. 408, no. 6808, pp. 50–50, 2000.

[10] D. M. Guldi and N. Martín, eds., *Carbon nanotubes and related structures: synthesis, characterization, functionalization, and applications.* John Wiley & Sons, 2010.

[11] X. Wang, Q. Li, J. Xie, Z. Jin, J. Wang, Y. Li, K. Jiang, and S. Fan, "Fabrication of ultralong and electrically uniform single-walled carbon nanotubes on clean substrates," *Nano Lett.*, vol. 9, no. 9, pp. 3137–3141, 2009.

[12] S. Bandow, S. Asaka, Y. Saito, A. M. Rao, L. Grigorian, E. Richter, and P. Eklund, "Effect of the growth temperature on the diameter distribution and chirality of single-wall carbon nanotubes," *Physical Review Letters*, vol. 80, no. 17, p. 3779, 1998.

[13] S. M. Bachilo, L. Balzano, J. E. Herrera, F. Pompeo, D. E. Resasco, and R. B. Weisman, "Narrow (n, m)-distribution of single-walled carbon nanotubes grown using a solid supported catalyst," *Journal of the American Chemical Society*, vol. 125, no. 37, pp. 11186–11187, 2003.

[14] J. N. Coleman, U. Khan, W. J. Blau, and Y. K. Gunko, "Small but strong: a review of the mechanical properties of carbon nanotube–polymer composites," *Carbon*, vol. 44, no. 9, pp. 1624–1652, 2006.

[15] R. Saito, M. Fujita, G. Dresselhaus, and u. M. Dresselhaus, "Electronic structure of chiral graphene tubules," *Appl. Phys. Lett.*, vol. 60, no. 18, pp. 2204–2206, 1992.

[16] J. W. G. Wildöer, L. C. Venema, A. G. Rinzler, R. E. Smalley, and C. Dekker, "Electronic structure of atomically resolved carbon nanotubes," *Nature*, vol. 391, no. 6662, pp. 59–62, 1998.

[17] T. W. Odom, J.-L. Huang, P. Kim, and C. M. Lieber, "Atomic structure and electronic properties of single-walled carbon nanotubes," *Nature*, vol. 391, no. 6662, pp. 62–64, 1998.

[18] B. Q. Wei, R. Vajtai, P. M. Ajayan, *et al.*, "Reliability and current carrying capacity of carbon nanotubes," *Appl. Phys. Lett.*, vol. 79, no. 8, p. 1172, 2001.

[19] A. D. Franklin, M. Luisier, S.-J. Han, G. Tulevski, C. M. Breslin, L. Gignac, M. S. Lundstrom, and W. Haensch, "Sub-10 nm carbon nanotube transistor," *Nano Lett.*, vol. 12, no. 2, pp. 758–762, 2012.

[20] S. B. Desai, S. R. Madhvapathy, A. B. Sachid, J. P. Llinas, Q. Wang, G. H. Ahn, G. Pitner, M. J. Kim, J. Bokor, C. Hu, *et al.*, "$MoS_2$ transistors with 1-nanometer gate lengths," *Science*, vol. 354, no. 6308, pp. 99–102, 2016.

[21] D.-m. Sun, M. Y. Timmermans, Y. Tian, A. G. Nasibulin, E. I. Kauppinen, S. Kishimoto, T. Mizutani, and Y. Ohno, "Flexible high-performance carbon nanotube integrated circuits," *Nat. Nanotech*, vol. 6, no. 3, pp. 156–161, 2011.

[22] H. Wang, P. Wei, Y. Li, J. Han, H. R. Lee, B. D. Naab, N. Liu, C. Wang, E. Adijanto, B. C.-K. Tee, *et al.*, "Tuning the threshold voltage of carbon nanotube transistors by n-type molecular doping for robust and flexible complementary circuits," *PNAS*, vol. 111, no. 13, pp. 4776–4781, 2014.

[23] Q. Cui, F. Gao, S. Mukherjee, and Z. Gu, "Joining and interconnect formation of nanowires and carbon nanotubes for nanoelectronics and nanosystems," *Small*, vol. 5, no. 11, pp. 1246–1257, 2009.

[24] S. W. Lee, N. Yabuuchi, B. M. Gallant, S. Chen, B.-S. Kim, P. T. Hammond, and Y. Shao-Horn, "High-power lithium batteries from functionalized carbon-nanotube electrodes," *Nat. Nanotech*, vol. 5, no. 7, pp. 531–537, 2010.

[25] X.-M. Liu, Z. Dong Huang, S. Woon Oh, B. Zhang, P.-C. Ma, M. M. F. Yuen, and J.-K. Kim, "Carbon nanotube (CNT)-based composites as electrode material for rechargeable Li-ion batteries: a review," *Compos. Sci. Technol.*, vol. 72, no. 2, pp. 121–144, 2012.

[26] Y. Wang and J. T. Yeow, "A review of carbon nanotubes-based gas sensors," *J. Sens.*, vol. 2009, 2009.

[27] M. Mittal and A. Kumar, "Carbon nanotube (CNT) gas sensors for emissions from fossil fuel burning," *Sens. Actuators B*, vol. 203, pp. 349–362, 2014.

[28] C. B. Jacobs, M. J. Peairs, and B. J. Venton, "Review: Carbon nanotube based electrochemical sensors for biomolecules," *Anal. Chim. Acta*, vol. 662, no. 2, pp. 105–127, 2010.

[29] M. Holzinger, A. Le Goff, and S. Cosnier, "Nanomaterials for biosensing applications: a review," *Front. Chem.*, vol. 2, p. 63, 2014.

[30] A. Hashimoto, K. Suenaga, A. Gloter, K. Urita, and S. Iijima, "Direct evidence for atomic defects in graphene layers," *Nature*, vol. 430, no. 7002, pp. 870–873, 2004.

[31] H. Zhu, K. Suenaga, J. Wei, K. Wang, and D. Wu, "Atom-resolved imaging of carbon hexagons of carbon nanotubes," *J. Phys. Chem. C*, vol. 112, no. 30, pp. 11098–11101, 2008.

[32] J. M. Zuo, I. Vartanyants, M. Gao, R. Zhang, and L. A. Nagahara, "Atomic resolution imaging of a carbon nanotube from diffraction intensities," *Science*, vol. 300, no. 5624, pp. 1419–1421, 2003.

[33] L.-C. Qin, "Determination of the chiral indices (n, m) of carbon nanotubes by electron diffraction," *Phys. Chem. Chem. Phys.*, vol. 9, no. 1, pp. 31–48, 2007.

[34] A. Jorio, R. Saito, J. H. Hafner, C. M. Lieber, M. Hunter, T. McClure, G. Dresselhaus, and M. S. Dresselhaus, "Structural (n, m) determination of isolated single-wall carbon nanotubes by resonant Raman scattering," *Phys. Rev. Lett.*, vol. 86, no. 6, p. 1118, 2001.

[35] S. M. Bachilo, M. S. Strano, C. Kittrell, R. H. Hauge, R. E. Smalley, and R. B. Weisman, "Structure-assigned optical spectra of single-walled carbon nanotubes," *Science*, vol. 298, no. 5602, pp. 2361–2366, 2002.

[36] J. Lefebvre and P. Finnie, "Polarized photoluminescence excitation spectroscopy of single-walled carbon nanotubes," *Phys. Rev. Lett.*, vol. 98, no. 16, p. 167406, 2007.

[37] D. A. Tsyboulski, J.-D. R. Rocha, S. M. Bachilo, L. Cognet, and R. B. Weisman, "Structure-dependent fluorescence efficiencies of individual single-walled carbon nanotubes," *Nano Lett.*, vol. 7, no. 10, pp. 3080–3085, 2007.

[38] D. I. Levshov, H. N. Tran, M. Paillet, R. Arenal, X. T. Than, A. A. Zahab, Y. I. Yuzyuk, J.-L. Sauvajol, and T. Michel, "Accurate determination of the chiral indices of individual carbon nanotubes by combining electron diffraction and resonant Raman spectroscopy," *Carbon*, vol. 114, pp. 141–159, 2017.

[39] Y. Miyamoto, A. Rubio, S. Berber, M. Yoon, and D. Tománek, "Spectroscopic characterization of Stone-Wales defects in nanotubes," *Phys. Rev. B*, vol. 69, no. 12, p. 121413, 2004.

[40] J. Kotakoski, J. C. Meyer, S. Kurasch, D. Santos-Cottin, U. Kaiser, and A. V. Krasheninnikov, "Stone–Wales-type transformations in carbon nanostructures driven by electron irradiation," *Phys. Rev. B*, vol. 83, no. 24, p. 245420, 2011.

[41] P. T. Araujo, M. Terrones, and M. S. Dresselhaus, "Defects and impurities in graphene-like materials," *Mater. Today*, vol. 15, no. 3, pp. 98–109, 2012.

[42] M. Kabir and K. J. Van Vliet, "Kinetics of topological Stone–Wales defect formation in single-walled carbon nanotubes," *J. Phys. Chem. C*, vol. 120, no. 3, pp. 1989–1993, 2016.

[43] J. Song, H. Liu, Y. Guo, and K. Zhu, "Electronic structures of Stone–Wales defective chiral (6, 2) silicon carbide nanotubes: First-principles calculations," *Physica E*, vol. 74, pp. 198–203, 2015.

[44] Q. Lu and B. Bhattacharya, "Effect of randomly occurring Stone–Wales defects on mechanical properties of carbon nanotubes using atomistic simulation," *Nanotechnology*, vol. 16, no. 4, p. 555, 2005.

[45] K. I. Tserpes and P. Papanikos, "The effect of Stone–Wales defect on the tensile behavior and fracture of single-walled carbon nanotubes," *Compos. Struct.*, vol. 79, no. 4, pp. 581–589, 2007.

[46] S. Sharma, R. Chandra, P. Kumar, and N. Kumar, "Effect of Stone–Wales and vacancy defects on elastic moduli of carbon nanotubes and their composites using molecular dynamics simulation," *Comput. Mater. Sci.*, vol. 86, pp. 1–8, 2014.

[47] H. F. Bettinger, "The reactivity of defects at the sidewalls of single-walled carbon nanotubes: the Stone-Wales defect," *J. Phys. Chem. B*, vol. 109, no. 15, pp. 6922–6924, 2005.

[48] J. A. Robinson, E. S. Snow, S. C. Badescu, T. L. Reinecke, and F. K. Perkins, "Role of defects in single-walled carbon nanotube chemical sensors," *Nano Lett.*, vol. 6, no. 8, pp. 1747–1751, 2006.

[49] M. B. Nardelli, B. I. Yakobson, and J. Bernholc, "Mechanism of strain release in carbon nanotubes," *Phys. Rev. B*, vol. 57, no. 8, p. R4277, 1998.

[50] H. Jiang, X.-Q. Feng, Y. Huang, K. C. Hwang, and P. D. Wu, "Defect nucleation in carbon nanotubes under tension and torsion: Stone–Wales transformation," *Comput. Methods Appl. Mech. Eng.*, vol. 193, no. 30, pp. 3419–3429, 2004.

[51] K. Suenaga, H. Wakabayashi, M. Koshino, Y. Sato, K. Urita, and S. Iijima, "Imaging active topological defects in carbon nanotubes," *Nat. Nanotech*, vol. 2, no. 6, pp. 358–360, 2007.

[52] G. G. Samsonidze, G. G. Samsonidze, and B. I. Yakobson, "Energetics of Stone–Wales defects in deformations of monoatomic hexagonal layers," *Comput. Mater. Sci.*, vol. 23, no. 1, pp. 62–72, 2002.

[53] M. Sammalkorpi, A. V. Krasheninnikov, A. Kuronen, K. Nordlund, and K. Kaski, "Irradiation-induced stiffening of carbon nanotube bundles," *Nucl. Instrum. Methods Phys. Res. Sect. B Beam Interact. Mater. Atoms*, vol. 228, no. 1, pp. 142–145, 2005.

[54] A. V. Krasheninnikov, K. Nordlund, M. Sirviö, E. Salonen, and J. Keinonen, "Formation of ion-irradiation-induced atomic-scale defects on walls of carbon nanotubes," *Phys. Rev. B*, vol. 63, no. 24, p. 245405, 2001.

[55] J.-C. Charlier, "Defects in carbon nanotubes," *Acc. Chem. Res.*, vol. 35, no. 12, pp. 1063–1069, 2002.

[56] Y. Zhang, J. Zhang, and D. S. Su, "Substitutional doping of carbon nanotubes with heteroatoms and their chemical applications," *ChemSusChem*, vol. 7, no. 5, pp. 1240–1250, 2014.

[57] S. J. Kim, Y. J. Park, E. J. Ra, K. K. Kim, K. H. An, Y. H. Lee, J. Y. Choi, C. H. Park, S. K. Doo, M. H. Park, *et al.*, "Defect-induced loading of Pt nanoparticles on carbon nanotubes," *Appl. Phys. Lett.*, vol. 90, no. 2, p. 023114, 2007.

[58] T. F. T. Cerqueira, S. Botti, A. San-Miguel, and M. A. L. Marques, "Density-functional tight-binding study of the collapse of carbon nanotubes under hydrostatic pressure," *Carbon*, vol. 69, pp. 355–360, 2014.

[59] S. Ayissi, P. A. Charpentier, K. Palotas, N. Farhangi, F. Schwarz, and W. A. Hofer, "Preferential adsorption of $TiO_2$ nanostructures on functionalized single-walled carbon nanotubes: A DFT study," *J. Phys. Chem. C*, vol. 119, no. 27, pp. 15085–15093, 2015.

[60] H. Do and N. A. Besley, "Calculation of the vibrational frequencies of carbon clusters and fullerenes with empirical potentials," *Phys. Chem. Chem. Phys.*, vol. 17, no. 5, pp. 3898–3908, 2015.

[61] P. M. Tailor, R. J. Wheatley, and N. A. Besley, "An empirical force field for the simulation of the vibrational spectroscopy of carbon nanomaterials," *Carbon*, vol. 113, pp. 299–308, 2017.

[62] Z. Yao, J.-S. Wang, B. Li, and G.-R. Liu, "Thermal conduction of carbon nanotubes using molecular dynamics," *Phys. Rev. B*, vol. 71, no. 8, p. 085417, 2005.

[63] A. M. Rao, E. Richter, S. Bandow, B. Chase, P. C. Eklund, K. A. Williams, S. Fang, K. R. Subbaswamy, M. Menon, A. Thess, *et al.*, "Diameter-selective Raman scattering from vibrational modes in carbon nanotubes," *Science*, vol. 275, no. 5297, pp. 187–191, 1997.

[64] R. Saito, T. Takeya, T. Kimura, G. Dresselhaus, and M. S. Dresselhaus, "Raman intensity of single-wall carbon nanotubes," *Phys. Rev. B*, vol. 57, no. 7, p. 4145, 1998.

[65] J.-L. Sauvajol, E. Anglaret, S. Rols, and L. Alvarez, "Phonons in single wall carbon nanotube bundles," *Carbon*, vol. 40, no. 10, pp. 1697–1714, 2002.

[66] W. A. Saidi and P. Norman, "Probing single-walled carbon nanotube defect chemistry using resonance Raman spectroscopy," *Carbon*, vol. 67, pp. 17–26, 2014.

[67] F. Herziger, C. Tyborski, O. Ochedowski, M. Schleberger, and J. Maultzsch, "Double-resonant LA phonon scattering in defective graphene and carbon nanotubes," *Phys. Rev. B*, vol. 90, no. 24, p. 245431, 2014.

[68] J. Laudenbach, D. Schmid, F. Herziger, F. Hennrich, M. Kappes, M. Muoth, M. Haluska, F. Hof, C. Backes, F. Hauke, *et al.*, "Diameter dependence of the defect-induced Raman modes in functionalized carbon nanotubes," *Carbon*, vol. 112, pp. 1–7, 2017.

[69] S. Rols, Z. Benes, E. Anglaret, J. L. Sauvajol, P. Papanek, J. E. Fischer, G. Coddens, H. Schober, and A. J. Dianoux, "Phonon density of states of single-wall carbon nanotubes," *Phys. Rev. Lett.*, vol. 85, no. 24, p. 5222, 2000.

[70] D. A. Kislitsyn, J. D. Hackley, and G. V. Nazin, "Vibrational excitation in electron transport through carbon nanotube quantum dots," *J. Phys. Chem. Lett.*, vol. 5, no. 18, pp. 3138–3143, 2014.

[71] L. Vitali, M. Burghard, M. A. Schneider, L. Liu, S. Y. Wu, C. S. Jayanthi, and K. Kern, "Phonon spectromicroscopy of carbon nanostructures with atomic resolution," *Phys. Rev. Lett.*, vol. 93, no. 13, p. 136103, 2004.

[72] M. Vandescuren, H. Amara, R. Langlet, and P. Lambin, "Characterization of single-walled carbon nanotubes containing defects from their local vibrational densities of states," *Carbon*, vol. 45, no. 2, pp. 349–356, 2007.

[73] F. D. Natterer, Y. Zhao, J. Wyrick, Y.-H. Chan, W.-Y. Ruan, M.-Y. Chou, K. Watanabe, T. Taniguchi, N. B. Zhitenev, and J. A. Stroscio, "Strong asymmetric charge carrier dependence in inelastic electron tunneling spectroscopy of graphene phonons," *Phys. Rev. Lett.*, vol. 114, no. 24, p. 245502, 2015.

[74] S. K. Jain, G. T. Barkema, N. Mousseau, C.-M. Fang, and M. A. van Huis, "Strong long-range relaxations of structural defects in graphene simulated using a new semiempirical potential," *J. Phys. Chem. C*, vol. 119, no. 17, pp. 9646–9655, 2015.

[75] S. K. Jain, V. Juričić, and G. T. Barkema, "Structure of twisted and buckled bilayer graphene," *2D Materials*, vol. 4, no. 1, p. 015018, 2016.

[76] S. K. Jain, V. Juričić, and G. T. Barkema, "Boundaries determine the formation energies of lattice defects in two-dimensional buckled materials," *Phys. Rev. B*, vol. 94, no. 2, p. 020102, 2016.

[77] S. K. Jain, V. Juričić, and G. T. Barkema, "Probing the shape of a graphene nanobubble," *to be published*, 2016.

[78] J. Maultzsch, H. Telg, S. Reich, and C. Thomsen, "Radial breathing mode of single-walled carbon nanotubes: Optical transition energies and chiral-index assignment," *Phys. Rev. B*, vol. 72, no. 20, p. 205438, 2005.

[79] T. C. Dinadayalane and J. Leszczynski, "Stone–Wales defects with two different orientations in (5, 5) single-walled carbon nanotubes: a theoretical study," *Chem. Phys. Lett.*, vol. 434, no. 1, pp. 86–91, 2007.

[80] A. J. Pool, S. K. Jain, and G. T. Barkema, "Structural characterization of carbon nanotubes via the vibrational density of states," *to be published*, 2016.